Filamin depletion blocks endoplasmic spreading and destabilizes force-bearing adhesions

Christopher D. Lynch[a], Nils C. Gauthier[a,b], Nicolas Biais[a], Andre M. Lazar[a], Pere Roca-Cusachs[a], Cheng-Han Yu[b], and Michael P. Sheetz[a,b]

[a]Department of Biological Sciences, Columbia University, New York, NY 10027; [b]Mechanobiology Institute, National University of Singapore, Singapore 117411

ABSTRACT **Cell motility is an essential process that depends on a coherent, cross-linked actin cytoskeleton that physically coordinates the actions of numerous structural and signaling molecules. The actin cross-linking protein, filamin (Fln), has been implicated in the support of three-dimensional cortical actin networks capable of both maintaining cellular integrity and withstanding large forces. Although numerous studies have examined cells lacking one of the multiple Fln isoforms, compensatory mechanisms can mask novel phenotypes only observable by further Fln depletion. Indeed, shRNA-mediated knockdown of FlnA in FlnB$^{-/-}$ mouse embryonic fibroblasts (MEFs) causes a novel endoplasmic spreading deficiency as detected by endoplasmic reticulum markers. Microtubule (MT) extension rates are also decreased but not by peripheral actin flow, because this is also decreased in the Fln-depleted system. Additionally, Fln-depleted MEFs exhibit decreased adhesion stability that appears in increased ruffling of the cell edge, reduced adhesion size, transient traction forces, and decreased stress fibers. FlnA$^{-/-}$ MEFs, but not FlnB$^{-/-}$ MEFs, also show a moderate defect in endoplasm spreading, characterized by initial extension followed by abrupt retractions and stress fiber fracture. FlnA localizes to actin linkages surrounding the endoplasm, adhesions, and stress fibers. Thus we suggest that Flns have a major role in the maintenance of actin-based mechanical linkages that enable endoplasmic spreading and MT extension as well as sustained traction forces and mature focal adhesions.**

Monitoring Editor
Yu-Li Wang
Carnegie Mellon University

Received: Aug 4, 2010
Revised: Jan 18, 2011
Accepted: Feb 8, 2011

INTRODUCTION

Actin-based cell motility is exhibited in a number of distinct forms involving numerous structural and signaling molecules that provide the coordination needed to effect phenomena from development to cancer (Locascio and Nieto, 2001; Yamaguchi *et al.*, 2005). Motile mammalian fibroblasts depend mainly on the action of actin polymerization pushing against the cell membrane to drive extension (Pollard and Borisy, 2003), but myosin contraction is needed to maintain coherence (continuous, mechanical connectivity) through stimulation of actin filament formation at adhesions (Cai *et al.*, 2010; Rossier *et al.*, 2010) and to develop large forces on the matrix (Cai *et al.*, 2006). Focal adhesions and their precursors, focal contacts, physically link the matrix to the cell cytoskeleton and form the scaffold for numerous intracellular signaling pathways that involve cell–matrix interactions (Puklin-Faucher and Sheetz, 2009). Focal adhesions are large protein complexes formed on the ventral cell surface that are made up of numerous molecules, including integrins, talins, and filamins (Flns), among others that are involved in motility and signaling functions (Zaidel-Bar *et al.*, 2003).

The Flns have been implicated in numerous aspects of cellular shape and motility. Flns are ~280 kDa, ~80-nm-long protein monomers consisting of an N-terminal actin-binding domain followed by 24 immunoglobulin G–like domains that have the ability to homo- and heterodimerize (Hartwig and Stossel, 1975) and support the formation of three-dimensional actin networks (Hartwig and Shevlin, 1986; Gorlin *et al.*, 1990; Takafuta *et al.*, 1998; Flanagan *et al.*, 2001) as well as affect membrane–cytoskeleton interactions (Cunningham *et al.*, 1992). FlnA and FlnB are the two major Fln isoforms expressed

This article was published online ahead of print in MBoC in Press (http://www.molbiolcell.org/cgi/doi/10.1091/mbc.E10-08-0661) on February 16, 2011.

Address correspondence to: Michael P. Sheetz (ms2001@columbia.edu).

Abbreviations used: DIC, differential interference contrast; EGFP, enhanced green fluorescent protein; ER, endoplasmic reticulum; FL, full-length; Fln, filamin; FN, human plasma fibronectin; GFP, green fluorescent protein; MEF, mouse embryonic fibroblast; PBS, phosphate-buffered saline; PDMS, polydimethylsiloxane; RFP, red fluorescent protein; TIRF, total internal reflection fluorescence.

in fibroblasts (Stossel *et al.*, 2001), representing ~90% of total Fln levels (Baldassarre *et al.*, 2009). Recent rheological studies on Fln/actin gels have determined that Flns enable a high degree of resilience in actin networks (Kasza *et al.*, 2009a; Schmoller *et al.*, 2009), giving the cell the ability to form relatively soft actin networks at low Fln concentrations and bundle stress fibers at high Fln concentrations (Tseng *et al.*, 2004; Esue *et al.*, 2009). Flns also bind to integrins (Sharma *et al.*, 1995; Loo *et al.*, 1998). In fact, both Fln and talin bind to overlapping sites on integrins, and integrin phosphorylation can serve to modulate both talin and Fln binding (Kiema *et al.*, 2006; Takala *et al.*, 2008).

While FlnA-knockout mouse embryonic fibroblasts (MEFs) have shown minimal motility defects (Feng *et al.*, 2006), numerous studies on the FlnA-deficient M2 melanoma cell line have found extensive blebbing and motility-related defects (Cunningham *et al.*, 1992; Flanagan *et al.*, 2001), malformed actin architecture (Flanagan *et al.*, 2001), and the inability to sense external rigidity (Byfield *et al.*, 2009) and control cellular stiffness (Kasza *et al.*, 2009b). Additionally, Fln mutations can cause periventricular nodular heterotopia in humans, reflecting neuronal motility deficiencies (Fox *et al.*, 1998). In contrast, FlnB$^{-/-}$ MEFs have been reported to have motility defects and disrupted actin architecture (Zhou *et al.*, 2007). Importantly, there is high homology among Fln isoforms (Stossel *et al.*, 2001), and they appear to compensate for each other (Baldassarre *et al.*, 2009). Compensation between talin isoforms has been shown to mask dramatic phenotypes (Zhang *et al.*, 2008), and because talin and Fln share similar structural and functional roles in the cell, severe Fln depletion is likely to produce novel Fln-related phenotypes.

To better understand the functions of Fln, we have focused on the well-characterized process of cell spreading and polarization (Giannone *et al.*, 2007), during which a standard behavior can be reproducibly observed (Dubin-Thaler *et al.*, 2008). In that context, we found that a major defect emerged in the spreading of the central, organelle-rich endoplasm and the extension of microtubules (MTs) in Fln-depleted MEFs. Other characteristics during the late stages of spreading implicated Flns in the stabilization of longer-term adhesions and networks bridging cellular compartments.

RESULTS

Depletion of FlnA in FlnB$^{-/-}$ MEFs causes a spreading defect

FlnA levels were knocked down by transfecting FlnB$^{-/-}$ MEFs with an expression vector for FlnA-targeting shRNA, green fluorescent protein (GFP), and a puromycin resistance sequence. A nontargeting shRNA was similarly expressed as a negative control. GFP-expressing cells transfected with either vector were sorted from untransfected cells by fluorescence activated cell sorting (FACS) and subsequently lysed for Western blot analysis. Cells expressing the FlnA-targeting sequence showed an average of ~75% knockdown when compared with controls (Figure 1A). Additionally, representative immunofluorescence of the GFP-expressing cells with an antibody to FlnA showed an ~80–85% depletion of FlnA levels compared with controls in the same field (Figure 1D).

These Fln-depleted MEFs exhibited a spreading defect in that the central organelle-rich region was confined to a smaller area than it was in controls (Figure 1B). Furthermore the level of knockdown correlated with the level of condensation of the organelle-rich region (Figure 1D). The phenotype was rescued by expression of human FlnA-GFP in Fln-depleted MEFs (Figure 1C). Also, Fln-depleted MEFs exhibited a thicker central region than did controls (Figure 1E) by approximately a factor of 2 (Figure 1F).

Fln depletion blocks spreading of the endoplasm from the initiation of cell spreading

The spreading defect associated with Fln depletion appeared to be affecting the spreading of the endoplasm, a region previously described as the slightly raised region near the cell center containing the majority of membrane-bound organelles and surrounded by the ectoplasm, the peripheral region of dense actin arrays that exclude organelles (Nishizaka *et al.*, 2000). To confirm the molecular nature of this region, we transfected Fln-depleted MEFs and controls with a construct expressing a red fluorescent protein (RFP)-tagged endoplasmic reticulum (ER) marker, namely the calreticulin ER targeting sequence and the KDEL retention sequence. Fixation of transfected cells showed a smaller ER area in Fln-depleted MEFs (Figure 2B) compared with controls (Figure 2A). Because ER area is highly dependent on overall cell area, we measured the ratio of fluorescent ER area to differential interference contrast (DIC) whole cell area to determine the percentage of total area occupied by the ER. Fln-depleted MEFs exhibited an ~40% decrease in normalized ER area compared with controls (Figure 2C), confirming that Fln depletion causes a spreading defect of the ER. Importantly, we observed no significant difference between the area of Fln-depleted MEFs and controls, whereas the difference in ER areas was significant, even before normalization. Additionally, the vesicle-rich endoplasm was measured using video-enhanced DIC, and the area of the endoplasm was equal to the area of the ER (Figure 2C), showing that using DIC micrographs alone was suitable for analyzing ER area.

When viewed during early stages of spreading, Fln-depleted MEFs often had a particularly granular appearance in the periphery and showed increased ruffling (Figure 2E and Supplemental Movie 2) when compared with controls (Figure 2D and Supplemental Movie 1). The endoplasm also failed to spread. Normalized endoplasm areas of Fln-depleted cells were significantly decreased compared with controls independent of the time of spreading (Figure 2F).

MTs are confined in Fln-depleted MEFs

Because restriction of the ER to the cell center may result from the restriction of MTs (Waterman-Storer and Salmon, 1998) we stained Fln-depleted MEFs with anti-tubulin antibodies after 1 h on human plasma fibronectin (FN)-coated glass (Figure 3A). MTs in Fln-depleted MEFs were confined to the cell center compared with untransfected cells in the same field (Figure 3B). When the distance between the MT boundary and the cell edge was quantified, the MT boundary was twice as far from the edge in Fln-depleted MEFs as in controls in both total internal reflection fluorescence (TIRF) and epifluorescence (Figure 3, C and D). To determine whether MTs were only partially extending or if they were extending then retracting, we tracked MTs using fluorescent ensconsin (3xEMTB-GFP). MTs were constrained and did not extend to the cell edge during early stages of cell spreading (Figure 3, E and F).

MT restriction can occur due to either MT stabilization or abnormally rapid actin rearward flow. To determine whether MTs had become stabilized, time-lapse observations of EB3-RFP were performed. MTs in the Fln-depleted system exhibited lower growth rates than controls during the first 30 min of spreading (Figure 3G). Also, 50-μM blebbistatin treatment rescued Fln-depleted MT growth rates (Figure 3G). Additionally, actin rearward flow rates were measured from spreading initiation and during late spreading (>30 min) using LifeAct-Ruby (a gift from Roland Wedlich-Soldner, Max Planck Institute of Biochemistry, Martinsried, Germany). Rearward flow rates were significantly slower in Fln-depleted MEFs at early time

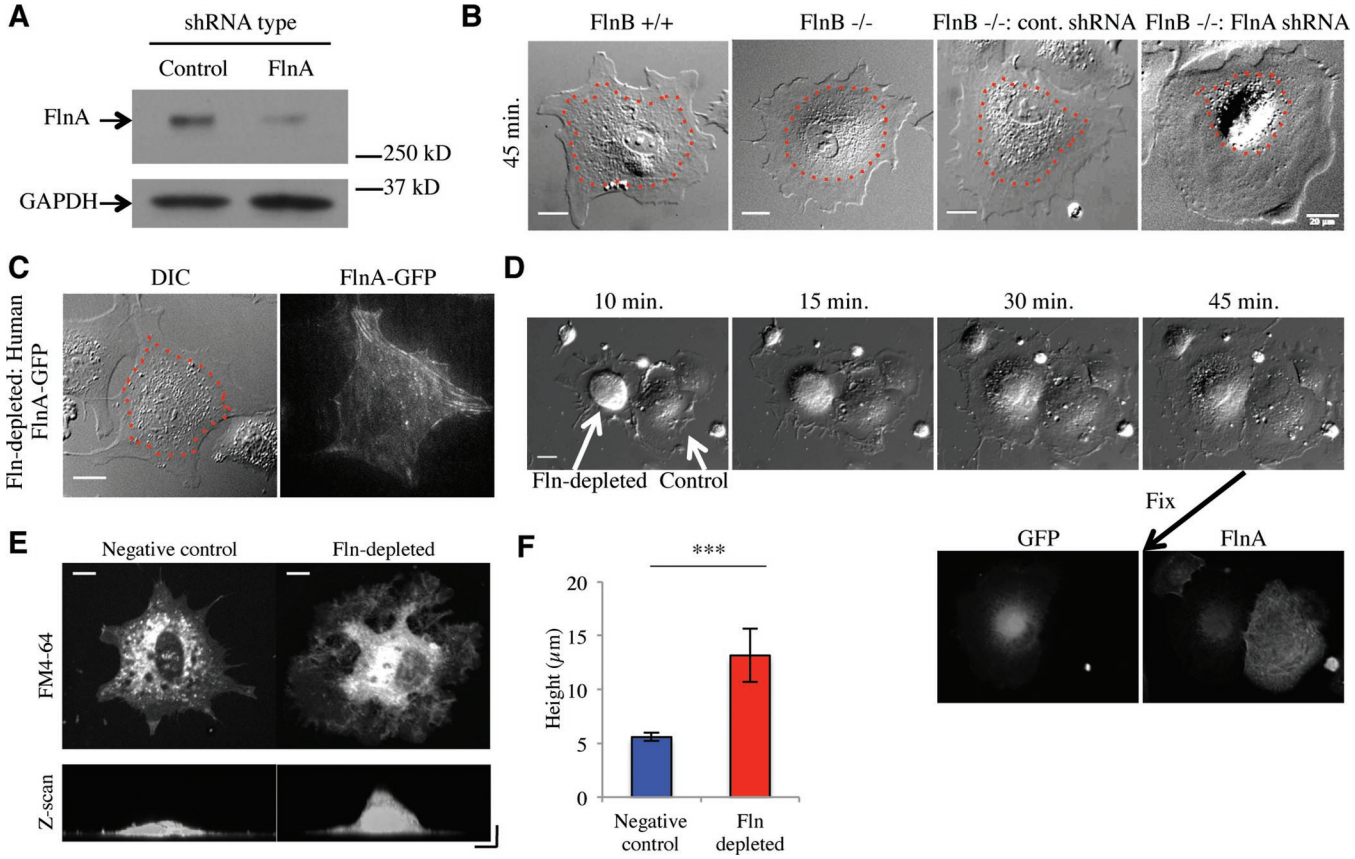

FIGURE 1: Fln depletion causes an early spreading defect. (A) Western blot of FlnB$^{-/-}$ MEFs transfected with nontargeting or FlnA-targeting shRNA vectors expressing GFP sorted from untransfected cells by FACS. FlnA levels were reduced 73% ± 5% (SEM) compared with the control (n = 3). (B) Cell lines were spread on FN-coated glass for 45 min and imaged. Endoplasmic regions are smaller in Fln-depleted MEFs compared with controls. Dotted red lines indicate endoplasmic regions. Scale = 20 μm. (C) Human FL FlnA-GFP rescued the endoplasmic spreading defect when transfected into Fln-depleted MEFs. Scale = 20 μm. (D) Fln-depleted MEFs (cell on left) exhibited an early spreading defect of the endoplasm when spread on 10 μg/ml FN-coated glass. Scale = 20 μm. The cells were fixed and immunostained for FlnA, resulting in correlation of GFP expression with FlnA knockdown and the endoplasmic spreading defect. (E) Fln-depleted and negative control MEFs were plated on 10 μg/ml FN-coated glass for 40 min and fixed. Cells were verified for GFP expression, treated with FM4-64 at 5 μg/ml in PBS for at least 5 min and imaged. Scale = 10 μm. Confocal z-scan along the *x*-axis of cells shown exhibits disparate thickness of endoplasmic region between Fln-depleted and control MEFs. Scale = 10 μm on both axes. (F) Quantification of cell heights over three separate experiments, at least 15 cells counted for cell type, ***$p < 0.001$.

points (Figure 3H), but at later times there was no difference between Fln-depleted MEFs and controls (Figure 3I).

Focal adhesions are small, transient, and unable to support edge extension in Fln-depleted MEFs

MT targeting is believed to be involved in focal adhesion dynamics (Kaverina *et al.*, 1999; Krylyshkina et al., 2002, 2003). Because MTs do not extend to the periphery in Fln-depleted cells, peripheral focal adhesions may also be altered. To test this possibility, Fln-depleted MEFs and untransfected controls were spread for 1 h and stained with anti-paxillin antibodies and phalloidin (Figure 4B). Fln-depleted cells exhibited small foci of paxillin accumulation and a disorganized actin cytoskeleton that was deficient in stress fibers compared with untransfected controls in the same field (Figure 4C). Because these controls were in fact FlnB$^{-/-}$ MEFs, it was important to examine FlnA localization in wild-type cells. We observed FlnA enrichment in several cytoskeletal structures, including transverse arcs surrounding the endoplasm, nodes of cross-linking connecting mature stress fibers extending above the endoplasm to the transverse arc ring below, as well as at the leading edge and the trailing ends of mature focal adhesions (Figure 4A). The smaller adhesions in Fln-depleted MEFs could be a result of less β1 integrin expression; however, this was found not to be the case (Figure 4D).

Because smaller adhesions could be explained by a deficiency in focal adhesion formation or unstable focal adhesions, we transfected Fln-depleted MEFs with paxillin-RFP and found that these cells formed focal contacts, but over time these contacts were unstable and were disassembled (Figure 4, E and F). When the lifetime of the contacts was measured for the Fln-depleted cells after onset of contraction, paxillin-RFP contacts had a much shorter lifetime (~8.5 min, SEM = 0.05 min, n = 45) compared with control adhesions that outlasted the time course of the experiment (>15 min). These results indicated that adhesions in Fln-depleted MEFs are more dynamic than those in controls. Because this finding suggests that these adhesions would not be able to support high levels of force, we induced contraction with the MT polymerization inhibitor nocodazole. Fln-depleted MEFs (Supplemental Movie 4) showed more

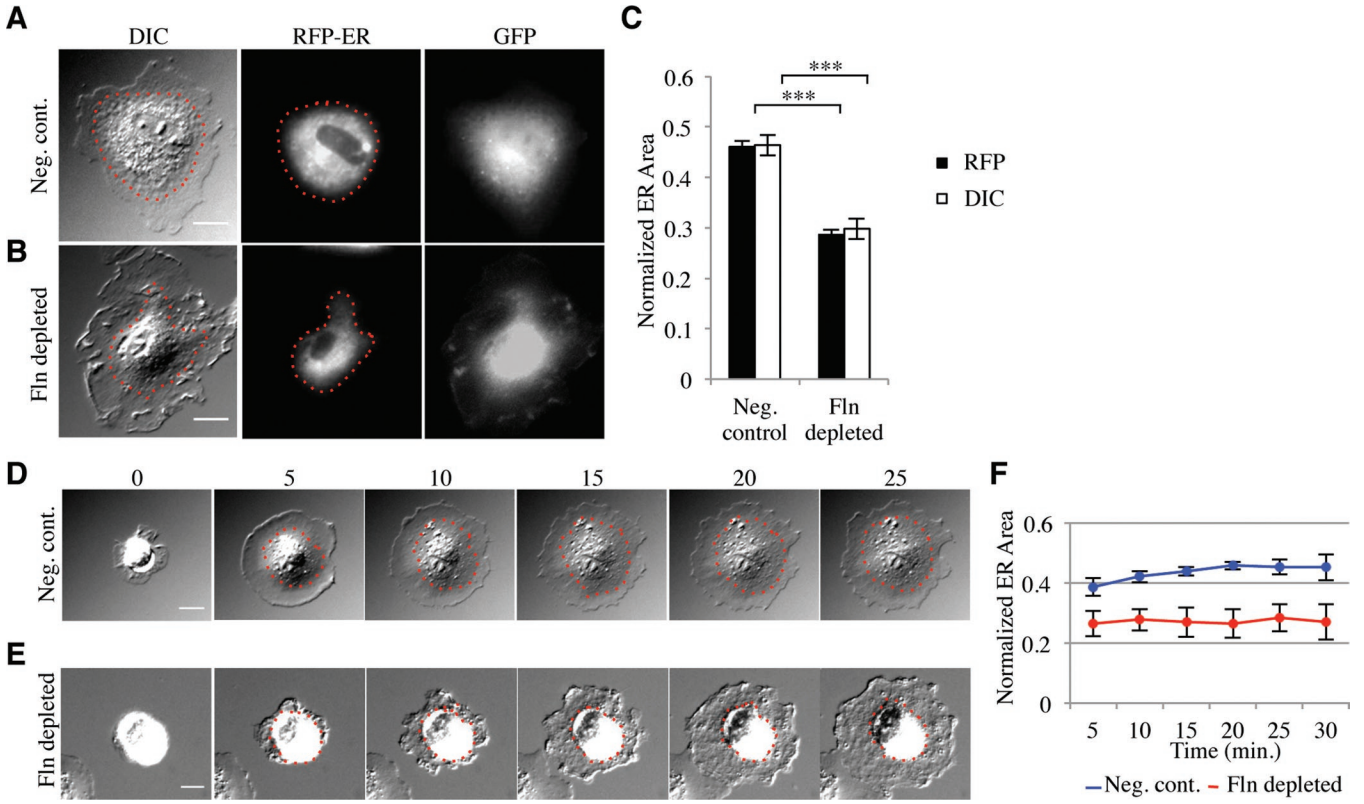

FIGURE 2: Fln depletion results in a reduction of ER spread area. (A) FlnB$^{-/-}$ MEFs transfected with negative control shRNA vector and RFP-ER were plated on FN-coated glass for 30 min and fixed. GFP signal served as a marker for shRNA transfection. Scale = 20 μm. (B) Same as in A, but transfected with FlnA-targeting shRNA. (C) ER area was measured by either RFP signal or DIC and normalized to the whole cell area as measured by DIC (***$p < 0.001$, $n = 44$). (D and E) Time-lapse images of negative control and Fln-depleted MEFs on FN. Scale = 20 μm. (F) Normalized endoplasm area over time ($n = 8$, $p < 0.001$).

rapid retraction of edge contacts and lamellipodial extensions, whereas controls (Supplemental Movie 3) even maintained narrow extensions (Figure 4G).

High forces are generated in Fln-depleted MEFs but rapidly release

Because unstable focal adhesions could result in defects of force generation, we measured the traction forces of Fln-depleted MEFs using an array of polydimethylsiloxane (PDMS) pillars (Tan *et al.*, 2003; du Roure *et al.*, 2005). When Fln-depleted MEFs were spread and imaged on PDMS pillars for ~30 min, they exhibited more narrow extensions than did controls (Figure 5, A and B). Representative force-versus-time traces from single-pillar measurements exhibited similar or higher levels of peak force generation (Figure 5, C and D); however, the release of force occurred at a higher rate in Fln-depleted cells when compared with controls (Figure 5E). In Fln-depleted cells, the average rate of force release was nearly four times that of controls (Figure 5F). Because this behavior could result from impaired traction force generation, we measured whole-cell force generation and found a slightly lower traction force per pillar in Fln-depleted MEFs, but the average value was not significantly different from controls (Figure 5G).

FlnA$^{-/-}$ cells have many characteristics of Fln-depleted cells

Given the dramatic motility defects in Fln-depleted MEFs, we asked whether these phenotypes could be attributed to either FlnA or FlnB. FlnA$^{-/-}$ MEFs exhibited a weaker ER spreading deficiency than did Fln-depleted MEFs (Figure 6A) (Supplemental Movie 5 for FlnA$^{+/+}$, Supplemental Movie 6 for FlnA$^{-/-}$) whereas FlnB$^{-/-}$ MEFs appeared similar to controls (Figure 1B). Averaged normalized ER areas of FlnA$^{-/-}$ (Figure 6B) but not FlnB$^{-/-}$ MEFs, were significantly decreased when compared with controls. Also, although FlnA$^{-/-}$ MEFs form stress fibers late in spreading, it was common for them to experience a contraction of the endoplasm that was not seen in controls or Fln-depleted MEFs. This contraction was often associated with stress fiber breakage and the appearance of gaps at the endoplasm boundary of FlnA$^{-/-}$ MEFs (Figure 6C and Supplemental Movie 7), suggesting that the cytoskeleton network was formed but was not able to sustain force at the endoplasm boundary. Stress fiber breakage was correlated with endoplasm retraction (Figure 6D), and gaps in the cytoplasm were observed at the endoplasm boundary of FlnA$^{-/-}$ MEFs (Figure 6E) during the contractile phase of spreading (Figure 6F).

Endoplasmic spreading requires the calpain-cleavability and integrin-binding functions of FlnA

To further understand Fln's role in the Fln-depleted endoplasmic spreading phenotype, Fln-depleted MEFs were transfected with RFP-ER and human full-length (FL) FlnA, calpain-uncleavable FlnA, or FlnA Δ19–21, the latter missing the primary integrin-binding site of FlnA. Normalized ER areas showed complete rescue of endoplasmic spreading upon FL FlnA addition, whereas calpain-uncleavable FlnA and FlnA Δ19–21 showed only partial rescue (Figure 7), indicating that both integrin binding and calpain cleavage play significant roles in Fln organization and function.

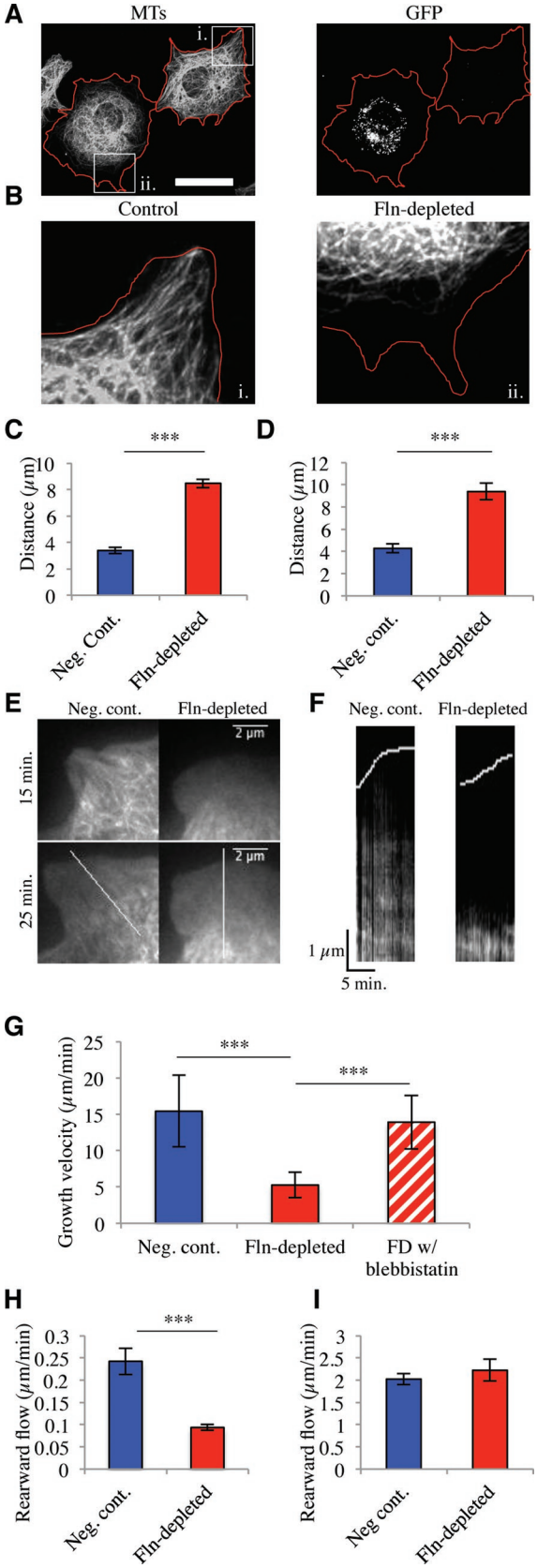

FIGURE 3: Fln depletion causes diminished MT extension in spreading MEFs. (A) FlnB$^{-/-}$ MEFs treated with FlnA shRNA were spread for 1 h on FN-coated glass, fixed, and stained for MTs. GFP-expressing cells were considered transfected and therefore Fln-depleted. Red lines demarcate cell edges. Scale = 50 μm. (B) Enlarged regions from A showing that Fln-depleted MEFs exhibit a larger distance between the MT boundary and the cell edge than do controls. (C) Quantification of distance from MT boundary to cell edge in Fln-depleted MEFs and controls after 15 min of spreading on FN-coated glass measured in TIRF (at least 10 measurements per cell, n = 3) (***p < 0.001). (D) Quantification of distance from MT boundary to cell edge in Fln-depleted and controls after 30 min of spreading on FN-coated glass measured with epifluorescence (at least 10 measurements per cell, n = 33) (***p < 0.001). (E) Fln-depleted MEFs and controls were transfected with 3x-ensconsin-GFP, allowed to spread, and imaged in TIRF. (F) Kymographs taken along white lines from E show a persistently larger distance between the MT boundary and the cell edge in Fln-depleted MEFs compared with controls. (G) Quantification of MT dynamics during the first 30 min of spreading by assessing EB3-RFP growth velocity. Fln-depleted MEFs exhibited slower MT extension than controls (multiple measurements per cell, n = 10 cells) (***p < 0.001), whereas 50 μM blebbistatin treatment rescued this phenotype (multiple measurements per cell, n = 7 cells) (***p < 0.001). (H) Quantification of actin rearward flow velocities by assessing LifeAct-Ruby dynamics from the initiation of spreading. Kymographs of Fln-depleted MEFs showed slower rearward flow than controls (multiple kymographs per cell, n = 6 cells/line) (***p < 0.001). (I) Rearward flow velocities gathered from cells spread for at least 30 min. Fln-depleted MEFs show no significant difference from controls (n = 11 cells/line).

DISCUSSION

Although previous studies of Fln isoform knockouts or mutants show interesting phenotypes (Cunningham *et al.*, 1992; Feng *et al.*, 2006; Zhou *et al.*, 2007), the depletion of multiple Flns shows a novel phenotype that as yet has not been ascribed to the loss of Flns: namely, a deficiency in endoplasmic spreading. Endoplasmic spreading refers to the flattening and subsequent increase in area of the central, membranous, organelle-rich region of the cell during cell spreading. A second region, the ectoplasm, surrounds the endoplasm and is depleted of organelles due to the presence of a dense actin network (Nishizaka *et al.*, 2000). When the spreading of the two regions is coupled, endoplasm area stabilizes at 50–60% of total cell area in controls (Figure 6B). The Fln-depleted deficiency in endoplasmic spreading results in a reduction of endoplasmic area to ~30% of total cell area (as assessed by a fluorescent ER marker) (Figure 2F) and is associated with a significant decrease in MT extension rate (Figure 3G). In addition, Fln-depleted cells lack stress fibers and have dynamic adhesions (Figure 4, B, C, E, and F). Although the traction forces generated by Fln-depleted cells are only slightly lower than those generated by control cells (Figure 5G), the rate of loss of tension is dramatically higher, indicating that Fln is important for maintaining mechanical forces on adhesions (Figure 5F). These changes are consistent with a role for Fln in stabilizing the actin cytoskeleton under force.

Because the ER typically spreads along MTs, it is expected that the MT arrays are condensed in Fln-depleted cells (Figure 3). This condensation was found to be partially due to the fact that MTs have lower extension rates in Fln-depleted MEFs than in controls (Figure 3G). Another possibility that has been shown previously (Terasaki and Reese, 1994) is that MT condensation could be a result of high rates of actin rearward flow preventing extension to the periphery. Rearward cortical actin flow rates were, however, actually lower in Fln-depleted MEFs than in controls during the period when MT extension rates were measured (Figure 3H) and not significantly higher than controls later in spreading (Figure 3I). The observation that blebbistatin treatment rescues MT condensation

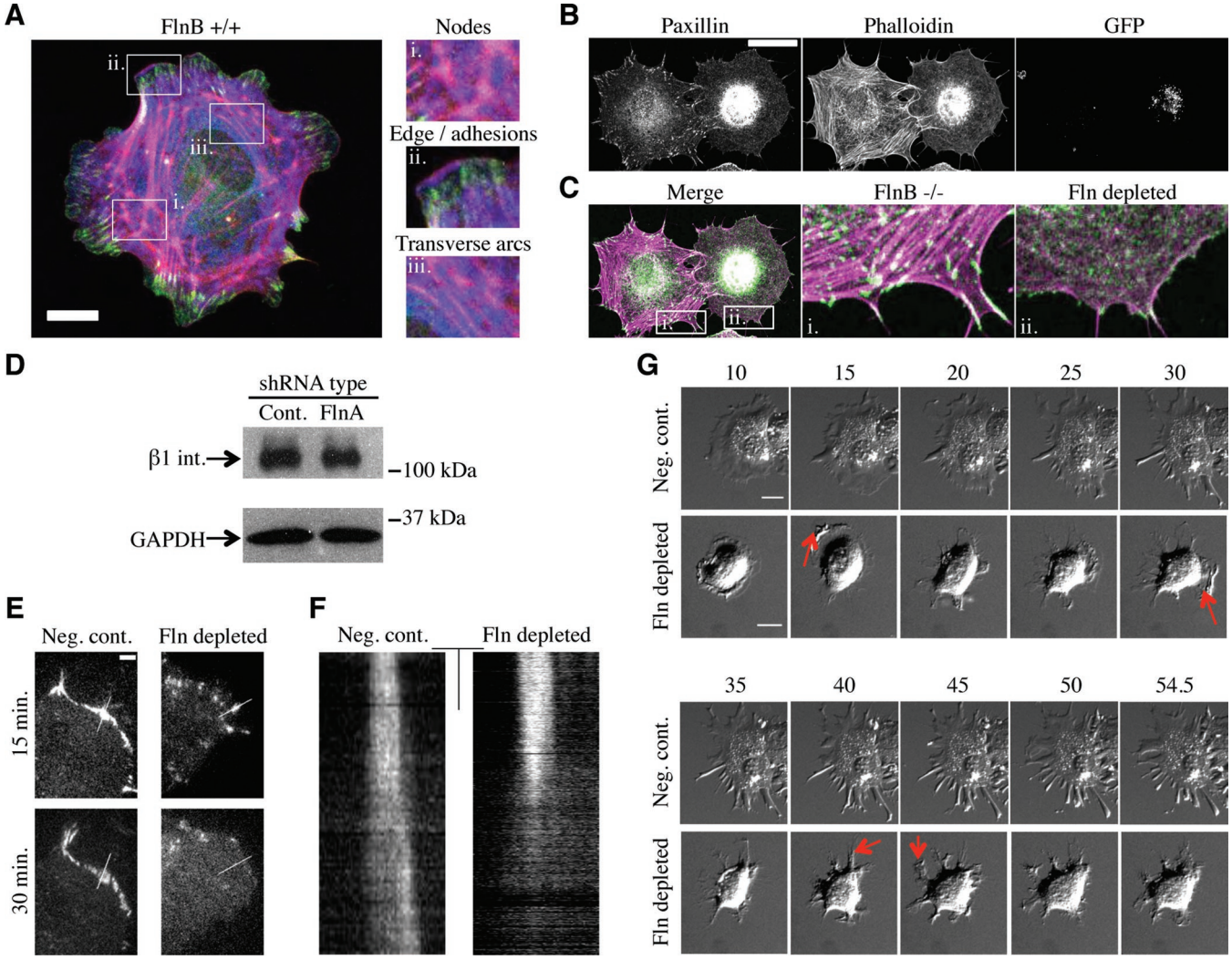

FIGURE 4: Fln depletion causes adhesion defects. (A) Merged confocal sections of FlnB$^{+/+}$ MEF 30 min after plating on FN-coated glass. Scale = 20 μm; green = paxillin, red = phalloidin, blue = FlnA). Enlarged regions highlight areas of FlnA enrichment, including large nodes at stress fiber junctions, the cell edge, adhesions, and transverse arcs surrounding the endoplasm. (B) FlnB$^{-/-}$ MEFs treated with FlnA shRNA were spread for 1 h on FN-coated glass, fixed, and stained for paxillin and phalloidin. GFP-expressing cells were considered transfected and therefore Fln-depleted. Scale = 50 μm. (C) Merged images of paxillin and F-actin panels show that Fln-depleted MEFs exhibited a highly disorganized, stress fiber-free, actin meshwork surrounding the endoplasm as well as a lack of focal adhesions compared with nontransfected cells. Scale = 50 μm; green pseudocoloring = paxillin, magenta = phalloidin). (D) FlnB$^{-/-}$ MEFs were transfected with nontargeting or FlnA-targeting shRNA expression vectors, sorted by FACS, and lysed. GFP-expressing cells from these populations exhibit no difference in beta 1 integrin expression. (E) Fln-depleted MEFs and controls expressing paxillin-RFP were spread on FN-coated glass and imaged with TIRF microscopy. Scale = 5 μm. (F) Kymographs taken along white lines in E show that focal adhesions do not retain their stability over the course of spreading in Fln-depleted MEFs. Scale = 5 μm; 3 min. (G) Fln-depleted MEFs and controls were trypsinized, resuspended in 10 μM nocodazole in serum-free DMEM for 30 min, and allowed to spread. Red arrows indicate protrusive regions that collapse in subsequent frames. Scale = 20 μm.

in Fln-depleted MEFs (Figure 3G) indicates that MT extension is hindered by a contractile actin network surrounding the endoplasm that, without Fln cross-linking, is presumably too dense to permit typical MT extension. As a result, MTs in Fln-depleted cells could potentially experience higher rates of catastrophe and pauses in growth.

This finding raises the question of whether the absence of MTs in the periphery would alter adhesion dynamics, membrane traffic, or other parameters. MTs are implicated in the process of adhesion turnover, but adhesions must form initially for this to occur. In the Fln-depleted cells, there is extensive ruffling of the edge that is indicative of a lack of stable adhesions in the periphery as is observed (Figure 4, B, C, E, and F) and perhaps an alteration in the process leading to mature stress fibers (Figure 4, B and C) (Hotulainen and Lappalainen, 2006). Furthermore the inability of the endoplasm to spread appears to precede the loss of early adhesions, which indicates that the primary defect is in adhesion maturation or in coupling of the MT ends to the peripheral adhesions to enable it to extend.

In considering adhesion maturation, it is useful to compare the adhesions that form after Fln depletion with the lack of even early adhesions after talin depletion. Fln-depleted cells formed early adhesions that quickly disassembled as indicated by RFP-paxillin

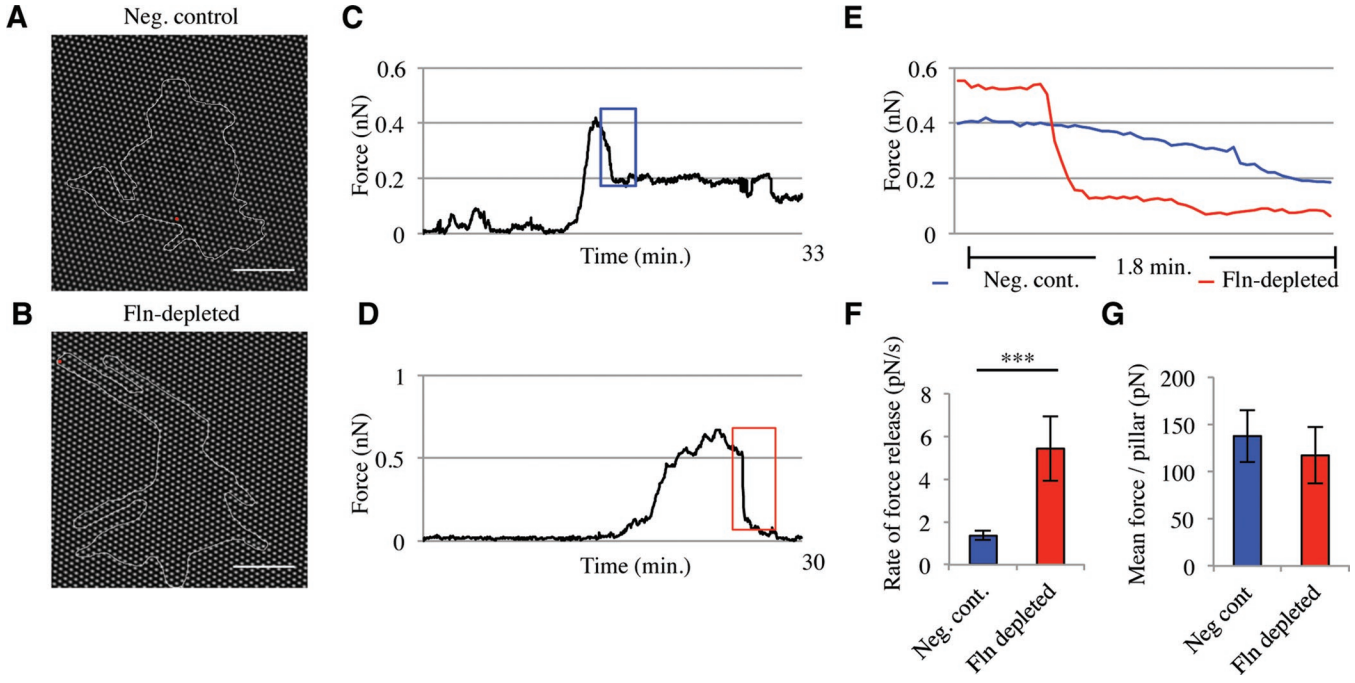

FIGURE 5: Fln-depleted MEFs exhibit an inability to sustain large, controlled forces on FN-coated pillars. (A and B) Fln-depleted MEFs and controls were spread on FN-coated PDMS pillars for ~30 min. Scale = 20 μm. (C and D) Representative traces of single pillar movements tracked over ~30 min of spreading in control (C) and Fln-depleted (D) MEFs (traces taken from pillars marked by a red dot in A and B). (E) Colored regions from C and D reveal rapid force release in Fln-depleted MEFs compared with controls. (F) Average rate of force-release events on pillars. Fln-depleted MEFs exhibited a significantly higher rate of force release compared with controls (5.42 pN/s ± 1.50 pN/s compared with 1.36 pN/s ± 0.21 pN/s, n = 29, ***$p < 0.001$). (G) Mean force/pillar of Fln-depleted MEFs and controls shows no significant difference in force generation capability (n = 12; >3 experiments).

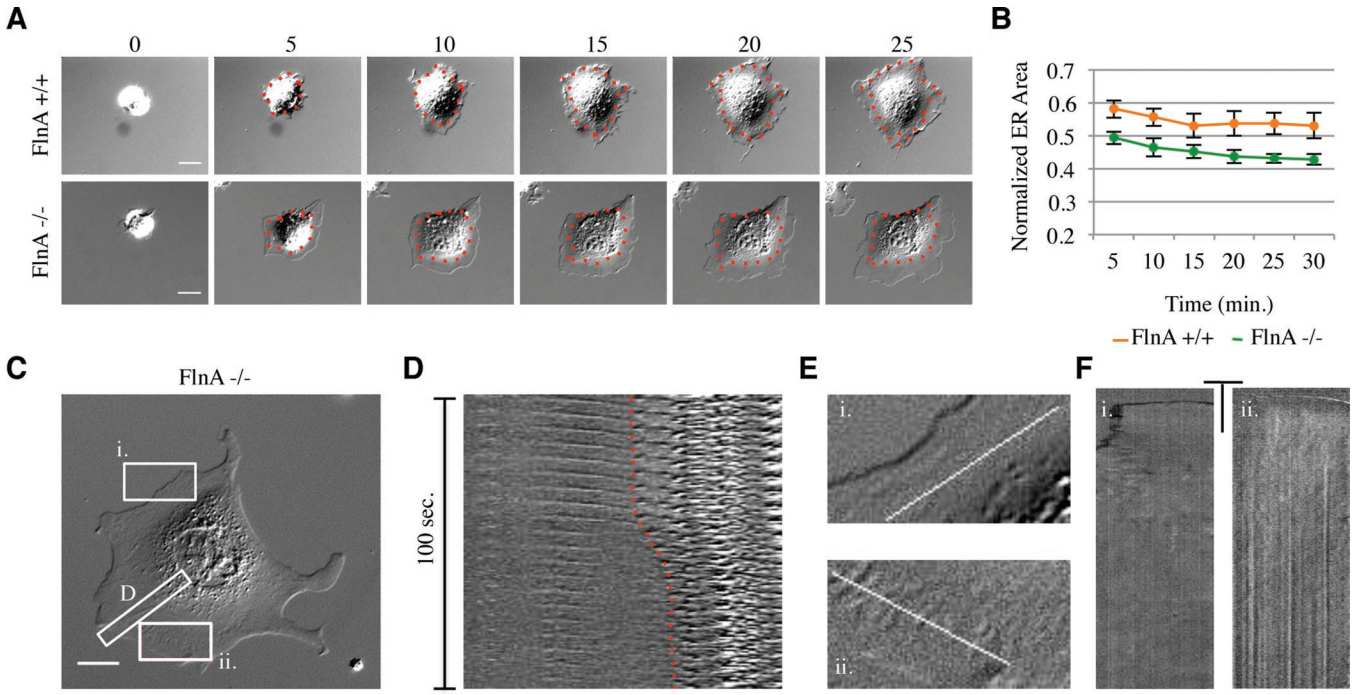

FIGURE 6: FlnA is the major Fln isoform involved in endoplasmic spreading defects. (A) Representative montages of single $FlnA^{+/+}$ and $FlnA^{-/-}$ MEFs spread for 25 min on FN (red dotted lines demarcate endoplasm regions). (B) Averaged normalized endoplasm areas for each cell line represented in A. Data shown are mean ± SEM (n = 17). Differences were significant throughout the time course ($p < 0.001$, two-way repeated measures ANOVA). (C) $FlnA^{-/-}$ MEF spread on FN-coated glass for 50 min. Scale = 20 μm. (D) Montage of stress fiber demarcated in C. After stress fiber breakage, the endoplasm is contracted rearward as indicated by red dotted line. (E) Enlarged images demarcated in A. Gaps are seen in ii., with a normal, coherent ectoplasm shown in i. for comparison. (F) Kymographs from lines seen in E. Gaps begin to appear 15 min after the initiation of spreading and persist throughout. Scale: 10 μm and 10 min.

dynamics (Figure 4, E and F). In contrast, talin-depleted MEFs did not exhibit extensive spreading or adhesion formation (Zhang *et al.*, 2008). We speculate that because Fln depletion appears to reduce the lifetime of adhesions, Fln may contribute to stabilization of adhesions and/or maintenance of the force-generating actomyosin network. Indeed, a recent study of Fln ligand-binding sites has shown Flns to have the capacity to bind multiple integrin beta tails at once, potentially allowing Fln to cluster integrins, and thereby replace talin in the formation of mature adhesions (Ithychanda *et al.*, 2009).

We found additional evidence that Fln is involved in stabilizing adhesions from the dynamics of force generation of Fln-depleted MEFs on PDMS pillars. Because many in vivo environments are discontinuous [there are micron-sized gaps in the cornea (Nishida *et al.*, 1988) and the intestinal mucosa (Toyoda *et al.*, 1997)], PDMS pillar arrays provide a relevant measure of cellular forces while still allowing for the accurate quantification of forces exerted by specific cellular regions (Tan *et al.*, 2003; du Roure *et al.*, 2005). The rate of force release on single pillars is approximately fourfold higher after Fln depletion compared with controls (Figure 5F). Whole-cell force measurements indicated a trend toward lower force exerted per pillar in the Fln-depleted system, although these findings were not significant (Figure 5G). Similar but stronger results were found using M2 cells (Kasza *et al.*, 2009b).

In the case of Fln-depleted fibroblasts, the presence of early adhesions, high traction forces, and rapid force release indicates that the matrix–integrin linkage to the cytoskeleton forms but is not sustained. As further support of this hypothesis, nocodazole treatment causes dramatic collapse of lamellipodial extensions in Fln-depleted MEFs (Figure 4G). Whether the collapse occurs at the level of the adhesion or the actin cytoskeleton is a subject for future studies, because Fln has roles in both stabilizing the actin cytoskeleton and linking integrins to actin filaments.

In addition to a role in traction force generation, Fln appears to play a structural role in stabilizing force-bearing structures within the cytoskeleton, because it is concentrated in interior regions of cytoplasm. The primary localization of FlnA is in structures surrounding the endoplasm both near the ventral surface and in nodes of cross-linked actin as well as in dorsal stress fibers (Figure 4A). Additionally, Fln appears to be found in the proximal regions of focal adhesions (Figure 4A), suggesting an important role in linking adhesions to the cytoskeleton proper. Accordingly, in time-lapse DIC movies of spreading FlnA$^{-/-}$ MEFs, we find stress fiber breakage that results in endoplasm retraction (Figure 6D and Supplemental Movie 7). We observe breakage events near adhesive contacts as well as in the middle of stress fibers, suggesting that the inability to sustain high levels of local force generation in Fln-depleted MEFs could be a result of weakness in both the dynamic actin cytoskeleton and the connections to adhesions.

It is logical that Flns may stabilize the structural linkages by spreading force among multiple actin filaments in dynamic cytoskeletal links within the actin network surrounding the endoplasm, in stress fibers, and in force-generating contacts on pillars. The observation that calpain-uncleavable FlnA and FlnA Δ19–21 do not completely rescue the endoplasmic spreading deficiency (Figure 7) supports this notion. In addition, Fln has an affinity for the membrane, as shown through the well-characterized blebbing of M2 melanoma cells (Cunningham *et al.*, 1992). Gaps in the membranes of FlnA$^{-/-}$ cells are indicative of that role as well (Figure 6, C, E, and F).

There appear to be two different roles for Fln in endoplasmic spreading (Figure 8). During the initial phases of spreading, the cortical cytoskeleton is flattened, which will cause the endoplasm to flatten as well. On the activation of contraction, the endoplasm will

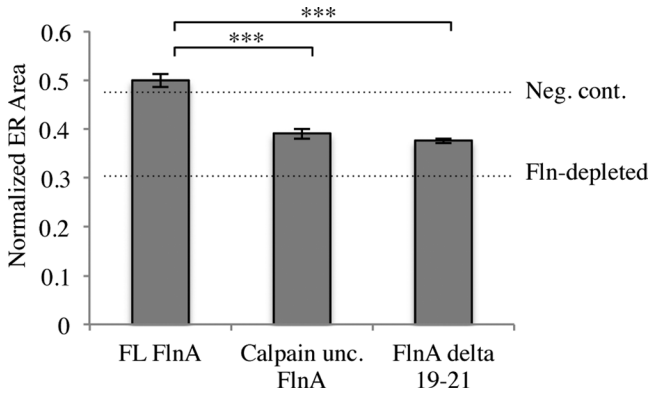

FIGURE 7: Calpain cleavability and integrin binding are FlnA functions critical in the ER spreading phenotype. Fln-depleted MEFs were transfected with RFP-ER and FL FlnA, calpain-uncleavable FlnA, or FlnA lacking domains 19–21. FL FlnA recovers the ER spreading phenotype to above control levels, whereas calpain-uncleavable FlnA and FlnA lacking domains 19–21 exhibit only partial recovery (n = 36) (***$p < 0.001$).

spread because of forces developed on the peripheral adhesions. In the absence of Fln, both mechanisms of spreading are weakened because of the loss of cross-links in the actin network. Connections between the endoplasm and surrounding cortical actin are particularly sensitive, explaining why gaps in the membrane form in this region in the FlnA$^{-/-}$ cells and why there are abrupt retractions of the endoplasmic boundary (Figure 6D). High forces generated within the contractile actin network surrounding the endoplasm that are normally transmitted through these connections would resist extension of MTs and the endoplasm boundary with the cell edge. This is still the case when calpain-uncleavable FlnA and FlnA Δ19–21 are added to the Fln-depleted system, underlining the importance of the Fln-adhesion linkage as well as the dynamic nature of actin cross-links (Figure 7).

Additionally, it should be noted that although our study concentrates on Fln-depleted and FlnA$^{-/-}$ MEFs, FlnB$^{-/-}$ MEFs did exhibit similar but less severe phenotypes. We suggest that the endoplasmic spreading deficiency that we report may be caused by a general Fln deficiency, rather than a deficiency of FlnA or FlnB specifically. Indeed FlnA and FlnB show high homology. However, FlnA typically comprises ~60% of expressed Flns in fibrosarcoma cells (Baldassarre *et al.*, 2009), indicating that loss of FlnA has a greater impact on cellular Fln levels than does loss of FlnB.

In summary, we suggest that the primary role of Flns during cell spreading is to stabilize the transmission of forces through adhesions to cross-linked and bundled actin structures to enable formation of a cohesive cytoskeleton that supports endoplasmic spreading and organelle dispersal. Although Fln itself may have no direct role in bearing tensile forces, its depletion results in major cytoskeletal disruptions as cells generate force. Furthermore Flns stabilize stress fibers and the actin cytoskeleton linkages to focal adhesions and membranes. Thus we suggest that the ER- and MT-rich cytoplasm behaves as a separate mechanical unit that is contractile and must be spread by pulling forces exerted on peripheral adhesions.

MATERIALS AND METHODS

Antibodies and membrane dyes

Fixable FM1–43x membrane dye and FM4–64 membrane dye were purchased from Molecular Probes (Eugene, OR). Rabbit polyclonal

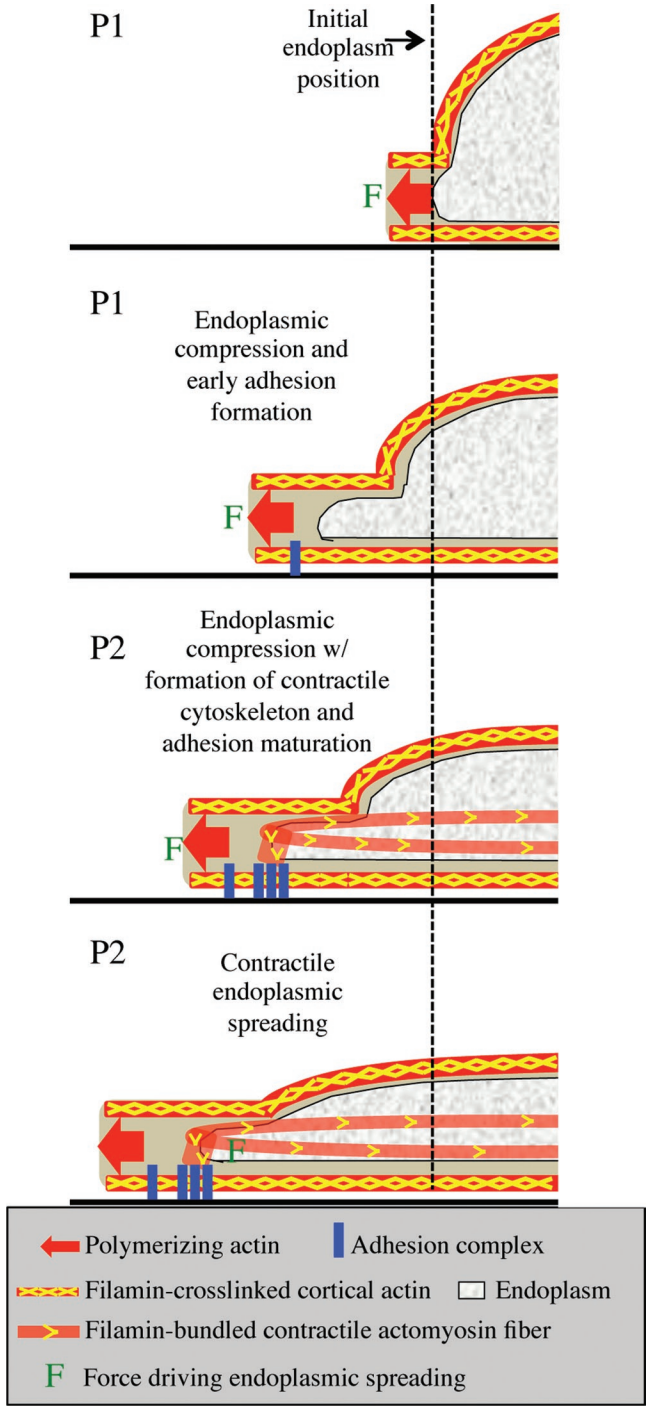

FIGURE 8: Schematic model of endoplasmic spreading. Initially the cell begins to spread via actin polymerization against the cell membrane. Cortical actin is cross-linked by Fln along the membrane. As the cell continues to spread, actin polymerization forces at the edge are transmitted back through the Fln-cross-linked cortex to the cell center, causing flattening of the endoplasm. At the same time, early adhesions begin to form. At the onset of contraction, cells exert contractile forces through mature focal adhesions, Fln-bundled actin stress fibers, and Fln-cross-linked actin meshworks (not shown for simplicity), allowing the endoplasm to spread in the direction of the edge despite being already flattened. Fln-depleted MEFs do not exhibit endoplasmic compression because they lack cortical cross-linking while they also do not experience contractile endoplasmic spreading due to unstable focal adhesions and a lack of strong actin stress fibers and cross-linked actin capable of stably supporting large forces exerted on the substrate.

anti-FlnA, mouse monoclonal anti-paxillin, mouse anti–beta-tubulin, mouse anti-GAPDH, and rhodamine-phalloidin were purchased from Novus Biologicals (Littleton, CO), BD Biosciences (Sparks, MD), Seven Hills Bioreagents (Cincinnati, OH), Santa Cruz Biotechnology (Santa Cruz, CA), and Molecular Probes, respectively.

Cell culture

FlnA$^{+/+}$, FlnA$^{-/-}$, FlnB$^{+/+}$, FlnB$^{-/-}$, and Fln-depleted MEFs were maintained in high-glucose DMEM (Life Technologies, Carlsbad, CA) + 10% fetal bovine serum (Life Technologies) at 37°C.

Constructs and transfection

pSilencer H1–3.1 puro expression vector (Ambion, Austin, TX) was used as described previously (Cai *et al.*, 2006) but targeting Mus musculus *flnA* with the sequence: 5′-CCATACTTACTGTATC-CGA-3′. Insert design was conducted using the pSilencer insert design tool on the Ambion Web site. For transfection detection, this vector was engineered to express GFP as well. pSilencer H1–3.1 puro-GFP bearing a nontargeting sequence was used as a control. pLNCX-paxillin-RFP was obtained from Michael Partridge (Columbia University, New York, NY). pEGFP-3xEMTB was obtained from Chloe Bulinski (Columbia University). pEGFP-filaminA and calpain-uncleavable FlnA-GFP was obtained from Donald Ingber (Children's Hospital and Harvard Medical School, Boston, MA). FlnA Δ19–21-GFP was obtained from David Calderwood (Yale University, New Haven, CT). RFP-EB3 was obtained from Richard Vallee (Columbia University). pRFP-ER was obtained from Clontech (Mountain View, CA). Transfection was accomplished using the Nucleofector system (Lonza, Walkersville, MD) or FuGENE HD transfection reagent (Roche, Basel, Switzerland). FlnB$^{-/-}$ MEFs were transfected according to the manufacturer's protocol, incubated for 1 d, exposed to puromycin at 1.75 μg/ml (Sigma, St. Louis, MO) in DMEM for 3 d, and used for experimentation.

FACS and Western blotting

Cells were transfected, allowed to recover for 1 d, exposed to puromycin at 1.75 μg/ml in DMEM for 3 d, trypsinized, and resuspended in serum-free DMEM. Samples were sorted by a FACSAria cell sorter (BD Biosciences), centrifuged, and lysed with RIPA buffer. After sonication, samples were stored at –80°C. SDS–PAGE and Western blotting were then performed as described previously (Zhang *et al.*, 2008).

Cover glass treatment and spreading assay preparation

On the day of the experiment, silanized cover glasses were treated with a droplet of FN (Roche) at 10 μg/ml and were incubated at 37°C for 1 h. Meanwhile, cells were trypsinized and resuspended in serum-free DMEM (without phenol red) (Life Technologies) for 30 min (for nocodazole studies, nocodazole was diluted in serum-free DMEM at 10 μM). Cells were then loaded into a sealed live-cell imaging chamber with an FN-coated cover glass on the bottom and an uncoated cover glass on top and spread at 37°C. DIC and epifluorescence microscopy were performed on an Olympus IX70 microscope (Center Valley, PA) mounted with a UPlanApo 20×, 0.70 NA objective (Olympus) and a Roper Scientific CoolSnap FX cooled CCD camera (Photometrics, Tucson, AZ), and TIRF microscopy was performed on an Olympus IX81 microscope with a PlanApo 60×, 1.45 NA oil immersion TIRF microscopy objective (Olympus) and a Cascade II camera (Photometrics). Imaging software was SimplePCI (Hamamatsu Corporation, Sewickley, PA).

Correlative cell-spreading assay with immunostaining

Cells were prepared as described earlier in the text but were loaded into a modified imaging chamber consisting of an FN-coated cover glass on the bottom, a circular rubber gasket in the middle, and an uncoated cover glass on top. Cells were then verified for GFP expression by epifluorescence microscopy and imaged with DIC microscopy for 45 min. Coated cover glass was then removed from the microscope, fixed and stained as described earlier in the text, and imaged once again to verify FlnA knockdown.

Immunostaining and FM1-43x/FM4-64 staining

Cells were fixed with 3.7% formaldehyde in phosphate-buffered saline (PBS), quenched with 50 mM ammonium chloride in PBS, and permeabilized with 0.1% Triton X-100 in PBS. Primary and secondary antibody stainings were performed at 37°C for 1.5 h each. Confocal imaging was completed on an Olympus IX81 microscope with a PlanApo 60×, 1.40 NA oil immersion objective and FluoView imaging software (Olympus). FM1-43x/FM4-64 staining was accomplished by briefly fixing cells with 7.4% (2×) formaldehyde followed by a 5-min incubation with FM1-43x/FM4-64 in 1× formaldehyde/PBS.

Quantification of distance between MT boundary and cell edge

Fln-depleted cells and their controls were transfected with 3×-ensconsin-GFP and allowed to spread. Distances between the MT boundary and cell edge were determined by drawing lines perpendicular to the cell edge from the edge to the MT boundary. At least 10 measurements were made per cell, and distances were measured using ImageJ (http://rsb.info.nih.gov/ij/).

Measurement of MT growth rates

EB3 signal was tracked using Nano Tracking plug-in for ImageJ (Nicolas Biais, Columbia University, referenced in Cai *et al.*, 2006, and Biais *et al.*, 2008). Displacement plots showed regions of growth, pause, and catastrophe. Regions of highest growth were analyzed for each cell type/condition in MATLAB (The MathWorks, Natick, MA).

Preparation of FN-coated PDMS pillars and force generation assays

PDMS was prepared in a 10:1 (wt/wt) ratio of PDMS/curing agent, placed in a vacuum chamber to remove bubbles, and molded over silicon wafers for 14 h at 65°C. Pillars were peeled in ethanol and quickly transferred to PBS. Pillars were then incubated at 37°C in FN at 10 μg/ml for 1.5 h for coating. After rinsing with PBS, cells were plated with CO_2-independent medium and imaged on coated pillars for ~30 min on an Olympus IX70 microscope mounted with a LUCPlanFl 40×, 0.60 NA objective (Olympus).

Image analysis and statistics

Analysis of Western blots was accomplished using the "Integrated Density" measurement in ImageJ. Endoplasm and whole cell areas of DIC images were measured by hand using the "Area" measurement in ImageJ. In some cells the endoplasm–ectoplasm boundary is easily identifiable with a still DIC image, but all of our measurements were performed on movies at the appropriate time point, making it easier to determine the endoplasm–ectoplasm boundary in DIC by tracking organelle movements. Kymographs were generated in ImageJ with the Multiple Kymograph function (J. Rietdorf and A. Seitz, European Molecular Biology Laboratory, Heidelberg, Germany). Analysis of force generation on PDMS pillars was completed using Nano Tracking. All other image processing was completed in ImageJ. All graphical data were completed in Excel 2008 (Microsoft, Redmond, WA) as was the execution of two-tailed Student's *t* tests and calculation of SD and SE values. Statistical analysis was done using SigmaStat (Systat, Chicago, IL) with two-tailed Student's *t* test when two cases were compared and with analysis of variance (ANOVA) tests when more comparisons were done. Line art was completed in Powerpoint 2008 (Microsoft).

ACKNOWLEDGMENTS

We thank Yuanyi Feng and Christopher Walsh for FlnA$^{+/+}$ and FlnA$^{-/-}$ MEFs, Xianghua Zhou and Levent Akyürek for FlnB$^{+/+}$ and FlnB$^{-/-}$ MEFs, Akiko Mammoto and Donald Ingber for the pEGFP-FlnA and calpain-uncleavable FlnA-GFP plasmid, J. Chloë Bulinski for the pEGFP-3xEMTB plasmid, Richard Vallee for the EB3-RFP plasmid, David Calderwood for the FlnA Δ19–21-GFP plasmid, and Michael Partridge for the pLNCX-paxillin-RFP plasmid. We also thank all past and present members of the Sheetz laboratory who assisted with our study, especially Simon Moore for critical readings of the manuscript. This work was supported by a National Institutes of Health training grant to C.D.L., NIH grant AI079030 to N.B., and NIH grant GM-03677–023 to M.P.S.

REFERENCES

Baldassarre M, Razinia Z, Burande CF, Lamsoul I, Lutz PG, Calderwood DA (2009). Filamins regulate cell spreading and initiation of cell migration. PLoS ONE 4, e7830.

Biais N, Ladoux B, Higashi D, So M, Sheetz M (2008). Cooperative retraction of bundled type IV pili enables nanonewton force generation. PLoS Biol 6, e87.

Byfield FJ, Wen Q, Levental I, Nordstrom K, Arratia PE, Miller RT, Janmey PA (2009). Absence of filamin A prevents cells from responding to stiffness gradients on gels coated with collagen but not fibronectin. Biophys J 96, 5095–5102.

Cai Y, Rossier O, Gauthier NC, Biais N, Fardin MA, Zhang X, Miller LW, Ladoux B, Cornish VW, Sheetz MP (2010). Cytoskeletal coherence requires myosin-IIA contractility. J Cell Sci 123, 413–423.

Cai Y *et al.* (2006). Nonmuscle myosin IIA-dependent force inhibits cell spreading and drives F-actin flow. Biophys J 91, 3907–3920.

Cunningham CC, Gorlin JB, Kwiatkowski DJ, Hartwig JH, Janmey PA, Byers HR, Stossel TP (1992). Actin-binding protein requirement for cortical stability and efficient locomotion. Science 255, 325–327.

du Roure O, Saez A, Buguin A, Austin RH, Chavrier P, Silberzan P, Ladoux B (2005). Force mapping in epithelial cell migration. Proc Natl Acad Sci USA 102, 2390–2395.

Dubin-Thaler BJ, Hofman JM, Cai Y, Xenias H, Spielman I, Shneidman AV, David LA, Dobereiner HG, Wiggins CH, Sheetz MP (2008). Quantification of cell edge velocities and traction forces reveals distinct motility modules during cell spreading. PLoS ONE 3, e3735.

Esue O, Tseng Y, Wirtz D (2009). Alpha-actinin and filamin cooperatively enhance the stiffness of actin filament networks. PLoS ONE 4, e4411.

Feng Y, Chen MH, Moskowitz IP, Mendonza AM, Vidali L, Nakamura F, Kwiatkowski DJ, Walsh CA (2006). Filamin A (FLNA) is required for cell-cell contact in vascular development and cardiac morphogenesis. Proc Natl Acad Sci USA 103, 19836–19841.

Flanagan LA, Chou J, Falet H, Neujahr R, Hartwig JH, Stossel TP (2001). Filamin A, the Arp2/3 complex, and the morphology and function of cortical actin filaments in human melanoma cells. J Cell Biol 155, 511–517.

Fox JW *et al.* (1998). Mutations in filamin 1 prevent migration of cerebral cortical neurons in human periventricular heterotopia. Neuron 21, 1315–1325.

Giannone G *et al.* (2007). Lamellipodial actin mechanically links myosin activity with adhesion-site formation. Cell 128, 561–575.

Gorlin JB, Yamin R, Egan S, Stewart M, Stossel TP, Kwiatkowski DJ, Hartwig JH (1990). Human endothelial actin-binding protein (ABP-280, nonmuscle filamin): a molecular leaf spring. J Cell Biol 111, 1089–1105.

Hartwig JH, Shevlin P (1986). The architecture of actin filaments and the ultrastructural location of actin-binding protein in the periphery of lung macrophages. J Cell Biol 103, 1007–1020.

Hartwig JH, Stossel TP (1975). Isolation and properties of actin, myosin, and a new actinbinding protein in rabbit alveolar macrophages. J Biol Chem 250, 5696–5705.

Hotulainen P, Lappalainen P (2006). Stress fibers are generated by two distinct actin assembly mechanisms in motile cells. J Cell Biol 173, 383–394.
Ithychanda SS, Hsu D, Li H, Yan L, Liu D, Das M, Plow EF, Qin J (2009). Identification and characterization of multiple similar ligand binding repeats in filamin: Implication on filamin-mediated receptor clustering and cross-talking. J Biol Chem 284, 35113–35121.
Kasza KE, Koenderink GH, Lin YC, Broedersz CP, Messner W, Nakamura F, Stossel TP, MacKintosh FC, Weitz DA (2009a). Nonlinear elasticity of stiff biopolymers connected by flexible linkers. Phys Rev E Stat Nonlin Soft Matter Phys 79, 041928.
Kasza KE, Nakamura F, Hu S, Kollmannsberger P, Bonakdar N, Fabry B, Stossel TP, Wang N, Weitz DA (2009b). Filamin A is essential for active cell stiffening but not passive stiffening under external force. Biophys J 96, 4326–4335.
Kaverina I, Krylyshkina O, Small JV (1999). Microtubule targeting of substrate contacts promotes their relaxation and dissociation. J Cell Biol 146, 1033–1044.
Kiema T, Lad Y, Jiang P, Oxley CL, Baldassarre M, Wegener KL, Campbell ID, Ylanne J, Calderwood DA (2006). The molecular basis of filamin binding to integrins and competition with talin. Mol Cell 21, 337–347.
Krylyshkina O, Anderson KI, Kaverina I, Upmann I, Manstein DJ, Small JV, Toomre DK (2003). Nanometer targeting of microtubules to focal adhesions. J Cell Biol 161, 853–859.
Krylyshkina O, Kaverina I, Kranewitter W, Steffen W, Alonso MC, Cross RA, Small JV (2002). Modulation of substrate adhesion dynamics via microtubule targeting requires kinesin-1. J Cell Biol 156, 349–359.
Locascio A, Nieto MA (2001). Cell movements during vertebrate development: integrated tissue behaviour versus individual cell migration. Curr Opin Genet Dev 11, 464–469.
Loo DT, Kanner SB, Aruffo A (1998). Filamin binds to the cytoplasmic domain of the beta1-integrinIdentification of amino acids responsible for this interaction. J Biol Chem 273, 23304–23312.
Nishida T, Yasumoto K, Otori T, Desaki J (1988). The network structure of corneal fibroblasts in the rat as revealed by scanning electron microscopy. Invest Ophthalmol Vis Sci 29, 1887–1890.
Nishizaka T, Shi Q, Sheetz MP (2000). Position-dependent linkages of fibronectin-integrin-cytoskeleton. Proc Natl Acad Sci USA 97, 692–697.
Pollard TD, Borisy GG (2003). Cellular motility driven by assembly and disassembly of actin filaments. Cell 112, 453–465.
Puklin-Faucher E, Sheetz MP (2009). The mechanical integrin cycle. J Cell Sci 122, 179–186.
Rossier OM *et al*. (2010). Force generated by actomyosin contraction builds bridges between adhesive contacts. EMBO J 29, 1055–1068.
Schmoller KM, Lieleg O, Bausch AR (2009). Structural and viscoelastic properties of actin/filamin networks: cross-linked versus bundled networks. Biophys J 97, 83–89.
Sharma CP, Ezzell RM, Arnaout MA (1995). Direct interaction of filamin (ABP-280) with the beta 2-integrin subunit CD18. J Immunol 154, 3461–3470.
Stossel TP, Condeelis J, Cooley L, Hartwig JH, Noegel A, Schleicher M, Shapiro SS (2001). Filamins as integrators of cell mechanics and signalling. Nat Rev Mol Cell Biol 2, 138–145.
Takafuta T, Wu G, Murphy GF, Shapiro SS (1998). Human beta-filamin is a new protein that interacts with the cytoplasmic tail of glycoprotein Ibalpha. J Biol Chem 273, 17531–17538.
Takala H, Nurminen E, Nurmi SM, Aatonen M, Strandin T, Takatalo M, Kiema T, Gahmberg CG, Ylanne J, Fagerholm SC (2008). Beta2 integrin phosphorylation on Thr758 acts as a molecular switch to regulate 14–3-3 and filamin binding. Blood 112, 1853–1862.
Tan JL, Tien J, Pirone DM, Gray DS, Bhadriraju K, Chen CS (2003). Cells lying on a bed of microneedles: an approach to isolate mechanical force. Proc Natl Acad Sci USA 100, 1484–1489.
Terasaki M, Reese TS (1994). Interactions among endoplasmic reticulum, microtubules, and retrograde movements of the cell surface. Cell Motil Cytoskeleton 29, 4291–300.
Toyoda H, Ina K, Kitamura H, Tsuda T, Shimada T (1997). Organization of the lamina propria mucosae of rat intestinal mucosa, with special reference to the subepithelial connective tissue. Acta Anat (Basel) 158, 172–184.
Tseng Y, An KM, Esue O, Wirtz D (2004). The bimodal role of filamin in controlling the architecture and mechanics of F-actin networks. J Biol Chem 279, 1819–1826.
Van Der Flier A, Sonnenberg A (2001). Structural and functional aspects of filamins. Biochim Biophys Acta 1538, 99–117.
Waterman-Storer CM, Salmon ED (1998). Endoplasmic reticulum membrane tubules are distributed by microtubules in living cells using three distinct mechanisms. Curr Biol 8, 798–806.
Yamaguchi H, Wyckoff J, Condeelis J (2005). Cell migration in tumors. Curr Opin Cell Biol 17, 559–564.
Zaidel-Bar R, Ballestrem C, Kam Z, Geiger B (2003). Early molecular events in the assembly of matrix adhesions at the leading edge of migrating cells. J Cell Sci 116, 4605–4613.
Zhang X, Jiang G, Cai Y, Monkley SJ, Critchley DR, Sheetz MP (2008). Talin depletion reveals independence of initial cell spreading from integrin activation and traction. Nat Cell Biol 10, 1062–1068.
Zhou X *et al*. (2007). Filamin B deficiency in mice results in skeletal malformations and impaired microvascular development. Proc Natl Acad Sci USA 104, 3919–3924.